IEEE Access
Multidisciplinary | Rapid Review | Open Access Journal

Received February 25, 2021, accepted March 3, 2021, date of publication March 12, 2021, date of current version March 24, 2021.

Digital Object Identifier 10.1109/ACCESS.2021.3065759

Design and Control of a Powered Lower Limb Orthosis Using a Cable-Differential Mechanism, COWALK-Mobile 2

JAEHWAN PARK[1,2], SEUNGHAN PARK[1], CHANKYU KIM[1], JONG HYEON PARK[2], (Member, IEEE), AND JUNHO CHOI[1], (Member, IEEE)

[1]Center for Bionics, Korea Institute of Science and Technology, Seoul 02792, South Korea
[2]School of Mechanical Engineering, Hanyang University, Seoul 04763, South Korea

Corresponding author: Junho Choi (junhochoi@kist.re.kr)

This work was supported by the Korea Institute of Science and Technology (KIST) Institutional Program under Project 2E31110.

ABSTRACT Powered lower limb orthoses have been commercially available for patients with Spinal Cord Injuries (SCI) or stroke. However, studies have shown that there are adverse effects on kinematics as well as metabolic energy of the users due to the additional mass of the orthoses to the lower limbs. Since additional metabolic energy required to use the powered orthoses is one of the reasons to avoid using them, it is important to reduce the mass and moment of inertia of the exoskeletons for longer use and better outcomes. In this study, a powered-lower-limb orthosis for stroke patients using a cable-differential mechanism, which is called COWALK-Mobile 2, was proposed. The cable-differential mechanism was utilized to transmit the actuating torques from actuators to the hip and knee joints. The cable-differential mechanism enabled the actuators to be located near the hip, which yields reduced inertia of the device, as well as the loads at the joints to be shared by the actuators, which results in smaller required actuator torque. Optimal radii of the pulleys for the cable-differential mechanism were found for efficient load-sharing during walking. Experimental results with a healthy person walking on a level surface have shown that larger joint torques were generated with smaller actuator torques.

INDEX TERMS Robotic orthosis, wearable robots, exoskeleton, differential mechanism.

I. INTRODUCTION

Powered lower limb orthoses are exoskeletal robotic devices for providing assisting torques to people having difficulties in walking, which are often caused by neuromuscular disorders or accidents. Their potential to be used for assistance or rehabilitation in walking has received attention from many researchers in the past few decades. For rehabilitation of children with cerebral palsy, Lerner *et al.* reported an exoskeleton to assist knee extension was effective in correcting a pathological gait pattern known as crouch gait [1], whereas Michmizos *et al.* integrated an exoskeleton with video games for ankle rehabilitation of children having cerebral palsy [2]. The impedance of an active ankle-foot orthosis was controlled throughout gait cycles to prevent drop-foot [3]. Quintero *et al.* developed an exoskeleton for patients with Spinal Cord Injuries (SCI), which assisted a paraplegic patient with sitting, standing, and walking [4]. Safety and feasibility of robotic orthoses in gait training for SCI patients have been treated in literatures [5]–[7]. Some orthoses developed for SCI patients are now on the market [8]–[11].

To assist walking, the joint torque and speed of a powered-lower-limb orthosis should cover the ranges of joint torque and speed needed by the user walking in the orthosis. To meet the requirements for the joint torque and speed, primarily heavy and bulky high-power actuators are necessary, resulting in increased mass and inertia of the device. However, increased mass and inertia of the device have adverse effects on kinematics [12], muscle activities [13], and metabolic energy expenditure of the users [14]. Studies have reported that excessive energy consumption required to wear them is responsible for abandoning the orthoses [15], [16]. Therefore, it is important to reduce the total weight of the actuators, which has a significant contribution to the weight and inertia of the device. In an effort to reduce the size and weight of the actuators on the exoskeletons, parallel elastic

The associate editor coordinating the review of this manuscript and approving it for publication was Pedro Neto.

actuators (PEA's) were used for an industrial exoskeleton designed to assist lifting heavy objects [17], [18] and an exoskeleton to help stroke patients with walking [19]. Because of the PEA's, reduced actuator torques were sufficient to assist walking and lifting due to the extra torques generated by the springs attached to the links in parallel to the actuators.

Since the location of the actuator also has significant contribution to the inertia of the device, for robotic manipulators, cable transmissions have been widely utilized to separate the actuators from the links [20], [21]. Many powered lower limb orthoses for indoor gait training used cables for remote control of joints with actuators on the ground [22]–[24] or on a cart [25]. Their exoskeleton became lighter due to the remote actuator, but the operating conditions were limited. Recently, better devices for assisting ground walking have been implemented with cables attached to lightweight rigid structures [26], [27] or soft braces [28]–[31], where the actuators are located on the back of the pelvis and minimal use of rigid structures reduces the mass and inertia of the device.

Unlike these devices which used cables for power transmission from the actuators to the joints of the devices, a cable-differential mechanism introduced by Park *et al.* in [32] enabled loads at the hip and knee joints to be shared by the actuators as well as locating the actuators near the hip joint. Reduction of the weight and inertia of the exoskeleton was feasible by the cable-differential mechanism. In this study, based on the results of Park *et al.*, an improved prototype of the powered-lower limb orthosis using a cable-differential mechanism for stroke patients is proposed and evaluated. For a better design of the orthosis, this paper aims to minimize the maximum torque and speed required for the actuators as well as improve the design and the control method. To this end, following improvements are made to the implemented orthosis.

1) The optimal pulley ratios of the cable-differential mechanism based on biomechanics of a human were found;
2) An actuated leg for the unaffected side were added;
3) A controller using the dynamics of the system were developed.

A biomechanics-based modification of the pulley ratio is described in Section II. System dynamics is derived, and a model-based controller for controlling the device is proposed in Section III. Experimental results are shown in Section IV, followed by conclusions in Section V.

II. A POWERED ORTHOSIS USING A CABLE-DIFFERENTIAL MECHANISM

The proposed powered lower limb orthosis in this paper, which is called COWALK-Mobile 2, is equipped with cable-differential mechanisms for power transmission. In this section, the basic design and working principle of COWALK-Mobile 2 are explained.

FIGURE 1. COWALK-Mobile 2.

A. DESIGN REQUIREMENTS OF COWALK-Mobile 2

When designing a powered orthosis with minimal negative effects on the user, it is desirable to meet the following design objectives:

1) The orthosis provides sufficient joint torques and angular speeds necessary for walking assistance;
2) The mass and inertia of the orthosis should be minimized to reduce any adverse effects on the user wearing the device.

The orthosis used in this research is designed for stroke patients, who often have capability to generate some portion of torques necessary for walking [33]. Therefore, the orthosis is designed to produce the rest of the torque needed by the users to walk. In this study, the level of assistance is set to be 60% for a user of 100kg.

Design specifications of the device were determined using the joint angular velocities and torques of a healthy male with weight of 56.7 kg while walking on the ground at $4.4\,\mathrm{km}\cdot\mathrm{h}^{-1}$, which was reported by Winter [34]. As shown in Fig. 2, it was reported that the maximum torques on the hip and knee joints are 54.4 N m and 37.8 N m, respectively. The maximum angular speed of the hip and knee joints are $3.49\,\mathrm{rad}\cdot\mathrm{s}^{-1}$ and $7.37\,\mathrm{rad}\cdot\mathrm{s}^{-1}$, respectively. Assuming the required torques are proportional to the weight of the user and 60% of the required torque at the joints are provided by the orthosis, the design specifications are set to be 57.57 N m for the hip joint and 40.0 N m for the knee joint.

Note that the maximum torque is required at the heel contact, while the maximum angular speed is required during the swing phase for each joint. Therefore, the mechanical power desired for each actuator is less than the product of its maximum torque and speed.

B. CABLE-DIFFERENTIAL MECHANISM

The cable-differential mechanism consists of two driving pulleys (pulleys A and B), one driven pulley (pulley C), and a connecting link (link D), as shown in Fig. 3. Pulley A is

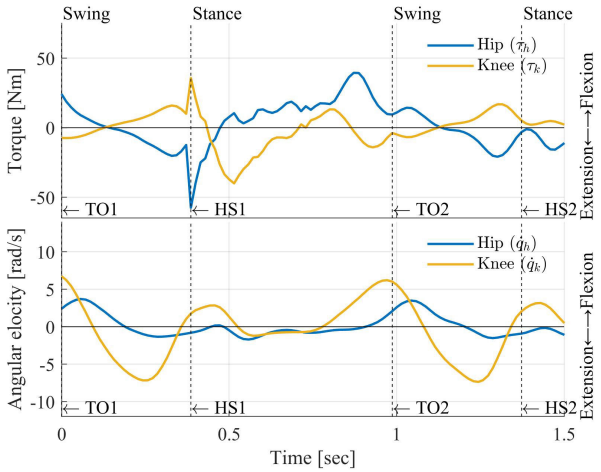

FIGURE 2. Joint angular velocities and torques of a healthy male walking on the ground at $4.4\,\mathrm{km}\cdot\mathrm{h}^{-1}$. The data is reproduced from [34]. Joint flexion is taken to be positive. (TO: Toe off, HS: Heel strike).

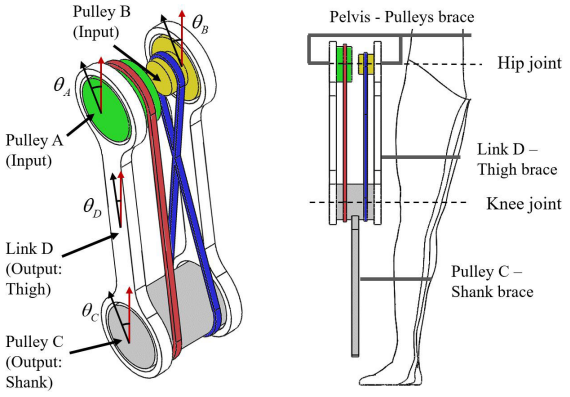

FIGURE 3. Concept of COWALK-Mobile 2. The driving pulleys are in line with the hip joint and the driven pulley is in line with the knee joint. θ_A, θ_B, θ_C, and θ_D are orientations of pulleys A, B, C, and link D, respectively. Input torques are applied at pulleys A and B..

connected to pulley C via a cable such that they rotate in the same direction. On the other hand, pulley B is connected to pulley C via another cable so that they rotate in the opposite directions. Then, their absolute angles are related by

$$\begin{aligned}(\theta_A - \theta_D) &= \gamma_a\,(\theta_C - \theta_D)\,,\\ (\theta_B - \theta_D) &= -\gamma_b\,(\theta_C - \theta_D)\,,\end{aligned} \tag{1}$$

where θ_A, θ_B, θ_C, and θ_D be the absolute angles of pulley A, B, C, and link D, respectively. γ_a is the ratio of the radius of pulley A to pulley C, and γ_b is the ratio between the radius of pulleys B and C.

In order for the cable-differential mechanism to be used in a powered orthosis, pulleys A and B are aligned with the hip joint, while pulley C is aligned with the knee joint. Link D is fixed to the thigh of the user with a brace. Shank link is connected to pulley C, to which the shank of the user is attached with a brace, as shown in Fig. 3. Then, flexion angle of the hip and knee, denoted by q_h and q_k respectively, are given as

$$\begin{aligned}q_h &:= \theta_D - \theta_u,\\ q_k &:= -\,(\theta_C - \theta_D)\,,\end{aligned} \tag{2}$$

where θ_u is the angle of the torso with respect to the inertial frame. The rotation angle of pulley A and B with respect to the torso, denoted by q_a and q_b respectively, are

$$\begin{aligned}q_a &:= \theta_A - \theta_u,\\ q_b &:= \theta_B - \theta_u.\end{aligned} \tag{3}$$

Assuming the cables are not stretchable, combining Eqs. (1), (2), and (3) yields the position of the joints as follows.

$$\begin{bmatrix} q_h \\ q_k \end{bmatrix} = \frac{1}{\gamma_a + \gamma_b}\begin{bmatrix} \gamma_b & \gamma_a \\ -1 & 1 \end{bmatrix}\begin{bmatrix} q_a \\ q_b \end{bmatrix}, \tag{4}$$

which implies this mechanism works as a differential mechanism. For example, under the assumption that the radii of the pulleys are identical, the hip joint moves at the average velocity of pulleys A and B, while the knee joint moves at the half of the velocity difference between pulleys A and B.

The torques of the joints and the pulleys are related by

$$\begin{bmatrix} \tau_h \\ \tau_k \end{bmatrix} = \begin{bmatrix} 1 & 1 \\ -\gamma_a & \gamma_b \end{bmatrix}\begin{bmatrix} \tau_a \\ \tau_b \end{bmatrix}, \tag{5}$$

where τ_h and τ_k are the flexion torques of the hip and knee joints and τ_a and τ_b are the torques of pulleys A and B, respectively. (See Appendix A for the derivations.) Eq. (5) illustrates that the loads at the joints are shared by two pulleys. For example, under the assumption that the radii of the pulleys are identical, torque of the hip is the sum of two pulley torques, and torque of the knee is the difference of two pulley torques, which implies that it is possible to generate greater joint torque by combining smaller torques generated by the actuators.

Furthermore, the cable-differential mechanism allows the actuators to be placed near the hip joints, which results in reduction of the inertia of the legs and the orthosis. Since reduced inertia of the orthosis results in less required torques for the actuators, it helps with reducing the torque requirements of the joints.

C. OPTIMAL GEAR RATIOS OF THE CABLE-DIFFERENTIAL MECHANISM

The required torques and angular velocities of the actuators attached to the driving pulleys are obtained using Eqs. (4) and (5), where the desired torques and velocities of the joints are obtained from Winter [34]. As shown in Eqs. (4) and (5), the required torques and angular velocities for the actuators change as γ_a and γ_b change. Therefore, it is desirable to find the pulley ratios to minimize the maximum torques and angular velocities required for the actuators.

Let $\dot{q}_{lim}$ and τ_{lim} be the angular speed and torque limitations of the selected actuator, respectively. These limitations usually come from mechanical or electromagnetic limitations

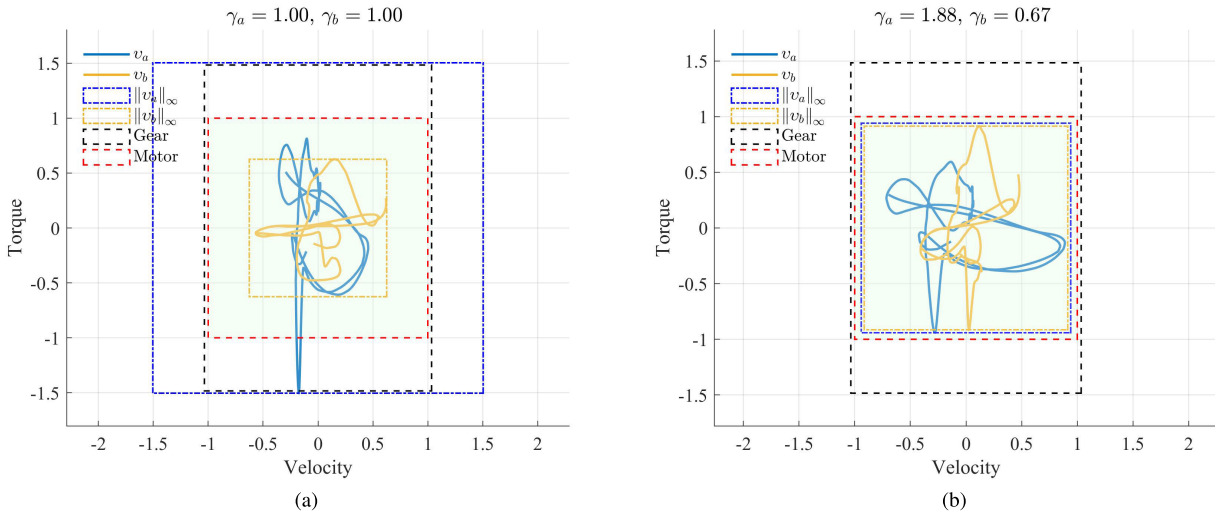

FIGURE 4. Trajectories of pulley A and B in the normalized angular velocity-torque space (υ_a and υ_b). (a) Gear ratio $\gamma_a = 1.0$ and $\gamma_b = 1.0$ are chosen. (b) The optimal gear ratio $\gamma_a = 1.88$ and $\gamma_b = 0.67$ are chosen. Angular velocities and torques are normalized by the limitations of the motor and gear.

of the electrical motor or gear reducer. Let υ_a and υ_b be the vectors of angular velocity and torque of pulleys A and B, normalized by the limitations of the actuators as follows.

$$\upsilon_a = \begin{bmatrix} \frac{\dot{q}_a(t)}{\dot{q}_{lim}} & \frac{\tau_a(t)}{\tau_{lim}} \end{bmatrix}^\top, \quad \upsilon_b = \begin{bmatrix} \frac{\dot{q}_b(t)}{\dot{q}_{lim}} & \frac{\tau_b(t)}{\tau_{lim}} \end{bmatrix}^\top, \quad (6)$$

where t is the gait phase ranging 0 to 1. To generate sufficient joint torques and speeds while avoiding saturations, it is desirable for the required torque-speed curve of the actuators to lie within the limitations of the actuators with maximum margins. Therefore, the maximum values of the normalized torques and speeds should be minimized. Let $\|\upsilon_a\|_\infty^{max}$ and $\|\upsilon_b\|_\infty^{max}$ be the maximum normalized torque and speed of each actuator over one gait cycle. Since minimizing $\|\upsilon_a\|_\infty^{max}$ and $\|\upsilon_b\|_\infty^{max}$ leads to the maximum margins, the optimal gear ratios are obtained by minimizing the cost function J described in the following optimization problem.

Find optimal gear ratios γ_a^* and γ_b^* such that

$$\gamma^* = \begin{bmatrix} \gamma_a^* & \gamma_b^* \end{bmatrix}^\top = \underset{\gamma_a>0, \gamma_b>0}{\arg\min} \; J(\gamma_a, \gamma_b), \quad (7)$$

where

$$J(\gamma_a, \gamma_b) = \|\upsilon_a\|_\infty^{max} + \|\upsilon_b\|_\infty^{max}, \quad (8)$$

for $\gamma_a > 0$ and $\gamma_b > 0$.

Note that if $\|\upsilon_a\|_\infty^{max} \leq 1$ and $\|\upsilon_b\|_\infty^{max} \leq 1$ are satisfied, the required torque and speed do not exceed the limitations of the actuator. However, if $\|\upsilon_a\|_\infty^{max} > 1$ or $\|\upsilon_b\|_\infty^{max} > 1$, the required torque or speed for the actuator exceeds the limit. The computed cost function is shown in Fig. 5 and the minimum of the cost function, which was obtained using *fmincon* function in MATLAB®, is found at $\gamma_a^* = 1.88$ and $\gamma_b^* = 0.67$. Fig. 4a shows the value of υ_a and υ_b with gear ratio $\gamma_a = \gamma_b = 1.0$ during walking, and Fig. 4b is when the optimal gear ratio of $\gamma_a = 1.88$ and $\gamma_b = 0.67$ are used. With the optimal gear ratios, the maximum values of the required angular speed and torque of the actuators lie within the boundaries, while the maximum required torque with gear ratios of 1:1 exceeds the limitation under the identical joint torque and speed requirements for both cases.

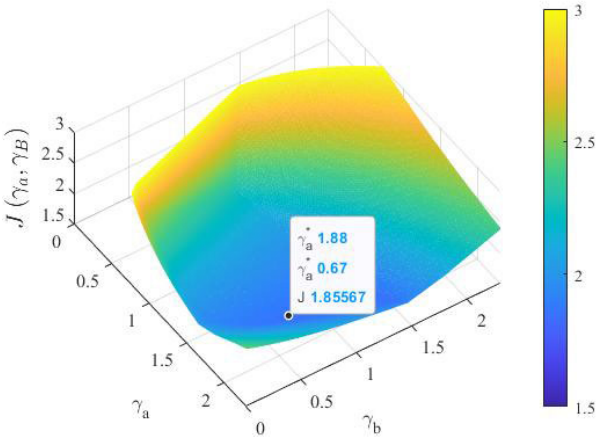

FIGURE 5. Computed cost function $J(\gamma_a, \gamma_b)$ for $\gamma_a > 0$ and $\gamma_b > 0$. The cost function has its minimum at $\gamma_a^* = 1.88$ and $\gamma_b^* = 0.67$.

D. IMPLEMENTED COWALK-Mobile 2

Implemented powered orthosis, which is called COWALK-Mobile 2, has two identical legs and a torso. Each leg has the hip, knee, and ankle joints. The hip and knee joints are actuated via the cable-differential mechanism, and the ankle joint is designed to be passive. All links of the orthosis are tied to the user using straps at the torso, thighs, shanks, and feet. Rigid foot brackets supporting the device are attached to the shoes using straps, see Fig. 6.

For implementation, two types of timing belts are used for power transmission from the driving pulleys to the driven

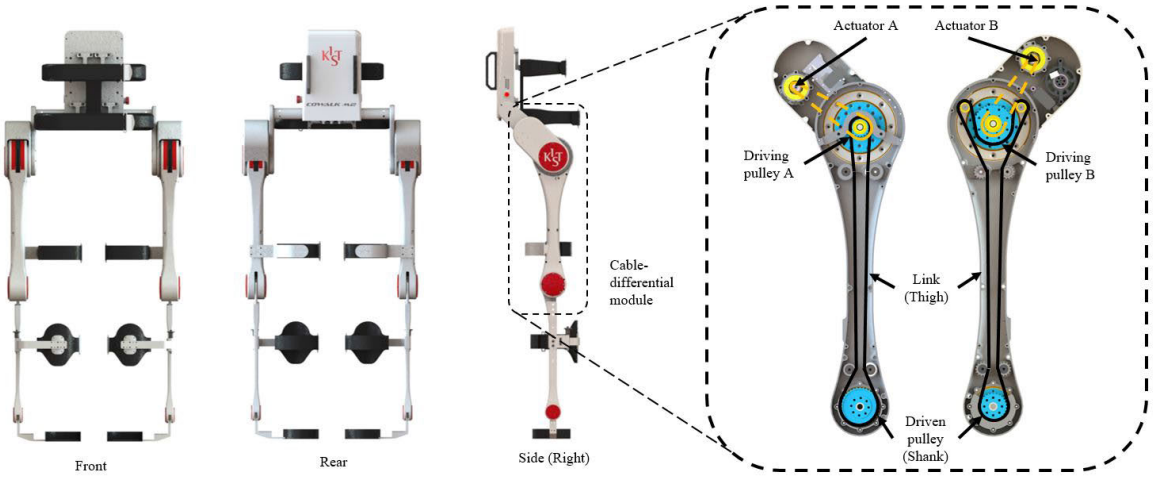

FIGURE 6. The design of the COWALK-Mobile 2. Cross-sectional view of the cable-differential module is shown on the right side. The solid lines in the cross-sectional view show the configurations of the timing belts. The driving pulley A and the driven pulley rotate in the same direction with single-sided timing belt, while the driving pulley B and the driven pulley rotate in the opposite direction with double-sided timing belt.

pulley instead of cable. Single-sided timing belt is used to preserve the direction of rotation of pulleys A and C whereas double-sided timing belt is used for opposite rotation of pulleys B and C. The ratios between the pulleys are selected to be $\gamma_a = 1.86$ and $\gamma_b = 0.64$ because they are the closest realizable pulley ratios using timing belts to the optimal solution. Each driving pulley is actuated by an identical electric BLDC motor (Kollmorgen, RBE00711C) via a harmonic gear (Harmonic drive, CSD-17-50), which has the gear ratio of 51:1. Each harmonic gear is connected to the electric motor using a timing belt with gear ratio of 2:1, resulting in a total gear ratio of 102:1.

The specifications of the device are listed in Table 1. The maximum torque of the hip joint is 62 N m and the knee joint is 78.12 N m, which are greater than maximum required torques. The weight of each leg module is 3.6 kg and center of mass is located at 19.37% of total leg length from the hip joint. To reduce the effect on the swing leg, the actuators are located close to the hip joint using the cable-differential mechanism. The total weight of the device is 14 kg including batteries and braces.

TABLE 1. Specifications of COWALK-Mobile 2.

Total weight	14 kg
The maximum torque of the hip joint	62 N m
The maximum torque of the knee joint	78.12 N m
The maximum torque of a driving pulley	31 N m
The maximum speed of a driving pulley	140 RPM
Nominal power of a driving pulley	99 W

Comparing with the cable-driven device by Lee *et al.* [26], which has maximum torque of 20 N m and weight of 14.5 kg, the implemented orthosis has larger maximum torque. The weight of COWALK-Mobile 2 is the same as HAL, which weighs 14 kg [10], and slightly heavier than Indego, which is 13.16 kg [11].

III. SYSTEM DYNAMICS AND DESIGN OF A CONTROLLER

A. DYNAMIC MODEL OF THE SYSTEM

Fig. 7 shows schematics of COWALK-Mobile 2 during the single-stance phase. Let $q_j := \left[q_u \; q_h^{st} \; q_k^{st} \; q_h^{sw} \; q_k^{sw}\right]^\top$ represent the joint coordinates, where q_u is the absolute angle of the torso, q_h and q_k are the angles of the hip and knee joints with the superscripts 'st' and 'sw' representing the stance and swing legs, respectively. Let $q_p := \left[q_a^{st} \; q_b^{st} \; q_a^{sw} \; q_b^{sw}\right]^\top$ represent the pulley coordinates. Then, the generalized coordinates are defined as

$$q := \left[q_j^\top \; q_p^\top\right]^\top. \tag{9}$$

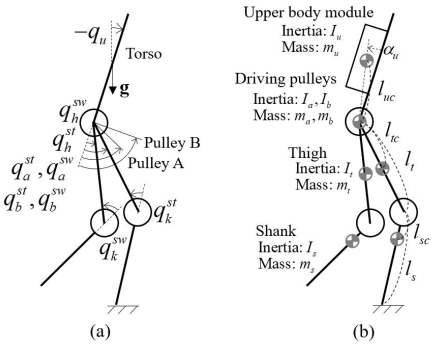

FIGURE 7. Schematics of COWALK-Mobile 2. (a) is the definition of the generalized coordinates, and (b) is the configurations and model parameters of the rigid bodies.

The governing dynamics of COWALK-Mobile 2 are obtained using the Euler-Lagrange method:

$$M(q)\ddot{q} + C(q,\dot{q})\dot{q} + G(q) + S(q) + F(\dot{q}) = \tau, \tag{10}$$

where $M(q)$ is the inertia matrix, $C(q,\dot{q})\dot{q}$ is the Coriolis-centrifugal force, $G(q)$ is the gravitational force, $S(q)$ is the torque caused by the compliance of the timing belts, $F(\dot{q})$ denotes the force due to the friction, and τ is the input torque. The equation of motion in Eq. (10) is decomposed as follows.

$$M_{jj}\ddot{q}_j + M_{jp}\ddot{q}_p + C_j + G_j + S_j = \tau_j, \tag{11}$$
$$M_{pj}\ddot{q}_j + M_{pp}\ddot{q}_p + S_p + F_p = \tau_p, \tag{12}$$

where $M_{jj} \in \mathbb{R}^{5\times5}$, $M_{jp} \in \mathbb{R}^{5\times4}$, $M_{pj} \in \mathbb{R}^{4\times5}$, and $M_{pp} \in \mathbb{R}^{4\times4}$ denote block matrices configuring inertia matrix, $C_j \in \mathbb{R}^5$ denotes the Coriolis and centrifugal torques of joints, $G_j \in \mathbb{R}^5$ denotes gravity term of joints, $S_j \in \mathbb{R}^5$ and $S_p \in \mathbb{R}^4$ denote the elastic torque at the joints and pulleys, respectively. Additionally, $F_p \in \mathbb{R}^4$ denotes the friction force, τ_j denotes the torques acting on the joints by interaction forces and other external disturbances, and τ_p denotes the torques of the actuators. (See Appendices B and C for details.)

The accelerations of the joints are calculated from Eq. (11):

$$\ddot{q}_j = {M_{jj}}^{-1}\left(-M_{jp}\ddot{q}_p - C_j - G_j - S_j - F_j + \tau_j\right). \tag{13}$$

Note that M_{jj} is a positive definite matrix. Plugging Eq. (13) into Eq. (12) yields

$$\begin{aligned}&\left(M_{pp} - M_{pj}{M_{jj}}^{-1}M_{jp}\right)\ddot{q}_p\\ &-M_{pj}{M_{jj}}^{-1}\left(C_j + G_j + S_j + F_j\right)\\ &+S_p + F_p = \tau_p - M_{pj}{M_{jj}}^{-1}\tau_j.\end{aligned} \tag{14}$$

Let us define matrices Λ and Ξ such that

$$\Lambda := M_{pp} - M_{pj}{M_{jj}}^{-1}M_{jp}, \tag{15}$$
$$\Xi := -M_{pj}{M_{jj}}^{-1}\left(C_j + G_j + S_j + F_j\right) + S_p + F_p, \tag{16}$$

respectively. Note that Λ is Schur complement of block M_{jj} in M and it is positive definite, i.e., Λ is positive definite since M is positive definite. Then, the pulley dynamics, Eq. (14), becomes

$$\Lambda\ddot{q}_p + \Xi = \tau_p - M_{pj}{M_{jj}}^{-1}\tau_j. \tag{17}$$

B. DESIGN OF A CONTROLLER

The desired gait patterns of the joints are used to obtain the desired trajectories of the driving pulleys. Let q_h^d and q_k^d be the desired positions of the hip and knee joints and let q_a^d and q_b^d be the desired pulley positions. Then, assuming no belt compliance, the desired pulley positions are calculated by Eq. (4) as follows.

$$\begin{bmatrix} q_a^d \\ q_b^d \end{bmatrix} = \begin{bmatrix} 1 & -\gamma_a \\ 1 & \gamma_b \end{bmatrix}\begin{bmatrix} q_h^d \\ q_k^d \end{bmatrix}. \tag{18}$$

In Eqs. (11) and (12), τ_p is the control input to the system, while τ_j is the external force and disturbances on the joints. Let us define control input of the pulley as follows.

$$\tau_p = \Xi + \Lambda\left(\ddot{q}_p^d - \sigma_d\left(\dot{q}_p - \dot{q}_p^d\right) - \sigma_p\left(q_p - q_p^d\right)\right), \tag{19}$$

where q_p^d is the desired position of the pulleys, σ_d and σ_p are control gains, and e is the position error, which is defined as $e := q_p - q_p^d$,. The error dynamics is

$$\frac{d}{dt}\begin{bmatrix} e \\ \dot{e} \end{bmatrix} = \begin{bmatrix} 0_{4\times4} & I_4 \\ -\sigma_p I_4 & -\sigma_d I_4 \end{bmatrix}\begin{bmatrix} e \\ \dot{e} \end{bmatrix} - \begin{bmatrix} 0_{4\times4} \\ I_4 \end{bmatrix} u, \tag{20}$$

where $u = \Lambda^{-1}M_{pj}{M_{jj}}^{-1}\tau_j$. Note that M_{pj} is a constant matrix and that u is bounded for bounded external joint torque τ_j. The control gain σ_d and σ_p should be selected such that the system matrix in Eq. (20) is *Hurwitz*. Then, the error dynamics is input-to-state stable.

C. IMPLEMENTATION OF THE CONTROLLER

The proposed controller is realized on a DSP (Texas Instrument, TMS 28377D) with 200 MHz system clock, see Fig. 8. The sampling frequency of the controller is 1 kHz. For feedback of the controller, each joint angle is measured by an absolute encoder (RLS, RMB28SC) and each actuator position is measured by a multi-turn absolute encoder (Heidenhain, EBI1135). The orientation of torso is measured by an IMU sensor (LORD, 3DM-GX4-25). For measurement of torque at each joint, a compact torque sensor (CAS KOREA, TQ-CSKG02-NM150) is implemented. Each driving pulley is actuated by a BLDC motor (Kollmorgen, RBE00711C) and its torque is estimated using actual quadrature axis (q-axis) current multiplied by the torque constant. The actuator position and torque data are acquired from a BLDC driver (ELMO motion control, G-WHI20/100SE) through CANopen protocol.

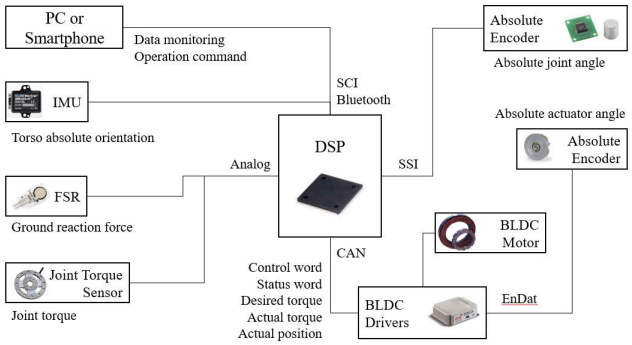

FIGURE 8. System diagram of COWALK-Mobile 2.

The measured foot pressure is used to determine which leg is in the stance phase. Two force sensitive resistors (Tekscan, FlexiForce®) are placed on the talus and the metatarsal of each foot. A leg is considered to be in stance when one of the pressures measured by the sensors on each leg exceeds a preset threshold.

IV. WALKING WITH COWALK-Mobile 2 AND THE RESULTS

To evaluate effectiveness of the cable-differential mechanism and performance of the proposed controller, an experiment to walk on a level surface wearing COWALK-Mobile 2 was

conducted. A healthy male subject (170 cm, 62 kg) walked straight in 118 strides wearing the device. Both legs of the device were controlled, and the subject was instructed to walk as passively as possible. The desired joint trajectories were obtained by scaling down the joint trajectories from Winter [34] by $4/5$ and adjusting the gait period to 1.41 s for a moderate walking pace, which was the preferred walking speed of the subject. The desired pulley trajectories are calculated using the kinematic equation in Eq. (18). The desired trajectories of left and right legs have phase difference of 50% gait cycle. The experimental protocol was approved by the Institutional Review Board (IRB) at the Korea Institute of Science and Technology.

The desired and actual positions of the hip and knee joints are shown in Fig. 9a. The trajectories are averaged over the gait cycles beginning with heel strikes. The joints track the desired positions with some position errors. In Fig. 9b, total position errors for the hip and knee joints as well as the position errors due to compliance of the belts used in the cable-differential mechanism are shown. The total position errors are defined as difference between the actual positions and the desired positions of the joints. The error due to compliance is defined as the difference between the actual joint positions and the expected joint positions calculated using the actual pulley positions assuming no compliance in the cables.

The hip joint was more flexed than the desired trajectory from mid-swing to mid-stance phase whereas more extended trajectory was observed from mid-stance to mid-swing phase. The knee joint showed more flexion except mid-swing phase where it showed more extended trajectory. As shown in Fig. 9b, compliance of the belts in the cable-differential mechanism is responsible for most of the position errors. Due to the gravity and compliance of the belts, flexed trajectory is observed at the knee joint during the stance phase. From mid-swing to mid-stance phase, the hip joint also showed more flexed trajectory than the desired because of the gravity and compliance. However, the hip joint have more extended trajectory from mid-stance to mid-swing phase.

Joint torques were measured with torque sensors and their average and standard deviation are shown at Fig. 9c. At the hip joint, extension torque was generated in the early-stance phase and in the late-swing phase whereas flexion torque was generated in the late-stance phase and in the early-swing phase. For the knee joint, flexion torque was generated at the heel strike and the late-swing phase. Extension torque was generated throughout the stance phase to the early-swing phase.

To see the effect of the proposed cable-differential mechanism, velocity-torque charts of the pulleys and the joints are shown in Fig. 10. As shown in Fig. 10b, the hip joint and the knee joint operated at relatively higher torque with relatively slower speed than those of the pulleys shown in Fig. 10a. This indicates high-speed operation of the pulleys are converted into high-torque operation of the joints due to the cable-differential mechanism. The maximum averaged

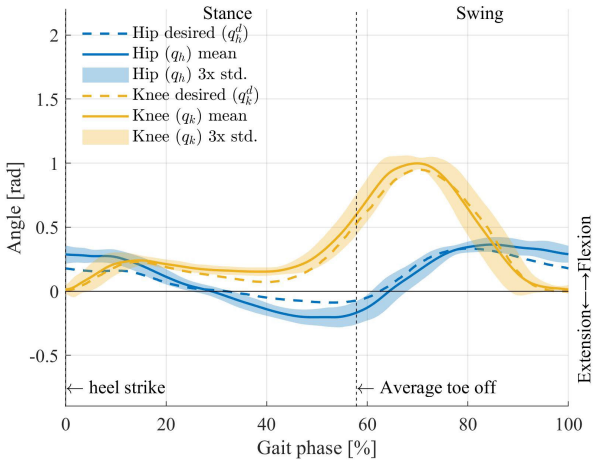

(a) Desired and actual trajectories of joints

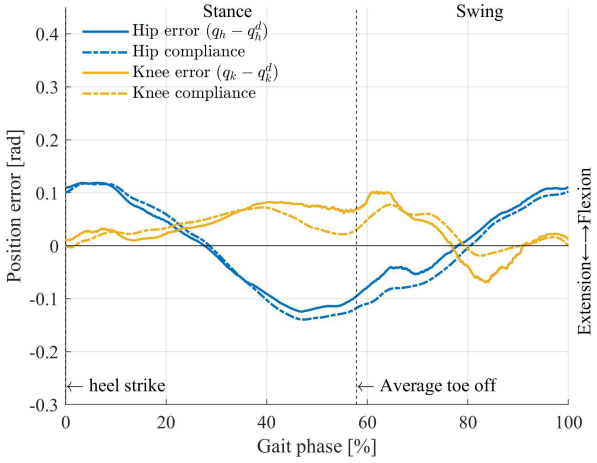

(b) Trajectory errors of joints

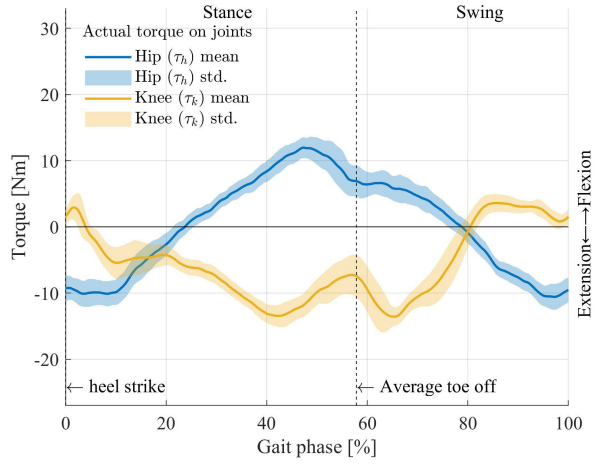

(c) Actual torques of joints

FIGURE 9. Experimental data of gait patterns and torques. Average and standard deviation of multiple gait cycle data are expressed graphically by solid lines and light-shaded shapes, respectively. The gait phase begins with the heel strike. Number of gait cycles is 118. Joint flexion is taken to be positive.

torque in the experiment for a single pulley is 8.09 N m, which is 26.1% of the maximum torque the device can produce. Since the maximum values of torque and speed of the pulleys are less than the limitations of the actuator, the device can

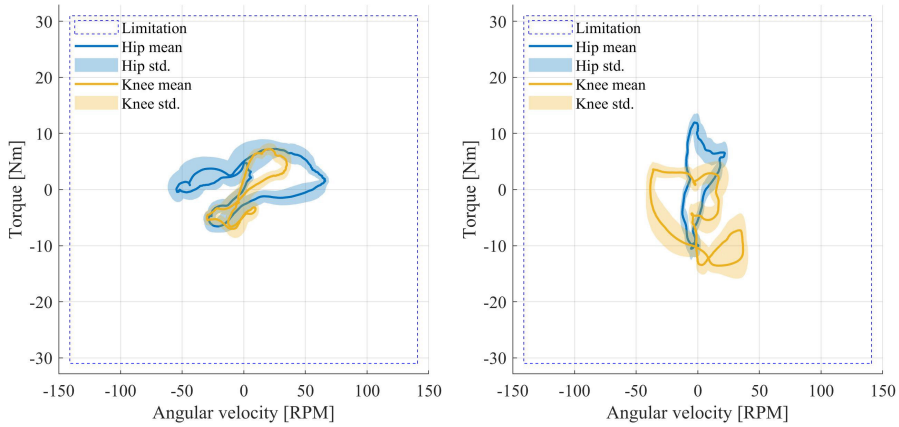

(a) Angular velocity-torque plot of the pulleys (b) Angular velocity-torque plot of the joints

FIGURE 10. Averaged velocity-torque trajectories of the pulleys and joints. Average and standard deviation of multiple gait cycle data are plotted with solid lines and light-shaded shapes, respectively. The standard deviation is represented in two dimensional space by an ellipsoidal shape at each phase of walking. Joint flexion is taken to be positive.

provide sufficient torques and speeds for walking. Note that it is also possible to use actuators with less torque and smaller margin.

V. CONCLUSION

In order to reduce the inertia of the swing leg and generate sufficient torques and speeds, a cable-differential mechanism was implemented for a powered-lower-limb orthosis, which is called COWALK-Mobile 2. The cable-differential mechanism allowed the load at the hip joint and the knee joint to be shared by two actuators located near the hip joint, which results in smaller inertia of the legs.

It was possible to change required torques and speeds of the actuators by changing the radius of the pulleys used in the cable-differential mechanism. The optimal radius of the pulleys was obtained solving an optimization problem with the biomechanical data of the human walking, and it was implemented to the design of the device. The proposed pulley controller based on the dynamics of the device was adapted for assistance of walking. An experiment of walking with the device has shown that larger joint torques were generated by smaller torques of the actuators while walking. Therefore, it was possible to design an orthosis with smaller actuators without degradation of performance, which lead to a lighter orthosis with higher torque.

In this research, the device was evaluated with an experiment involving a healthy subject. Further studies should be conducted to show the effectiveness of the device on rehabilitation of lower-limb functionality and metabolic energy consumption for stroke patients.

APPENDIX A
DERIVATION OF EQUATIONS IN THE CABLE-DIFFERENTIAL MECHANISM

Combining Eqs. (1), (2), and (3) yields

$$\begin{aligned} q_a &= q_h - \gamma_a q_k, \\ q_b &= q_h + \gamma_a q_k, . \end{aligned} \tag{21}$$

Then,

$$\begin{bmatrix} q_a \\ q_b \end{bmatrix} = \begin{bmatrix} 1 & -\gamma_a \\ 1 & \gamma_b \end{bmatrix} \begin{bmatrix} q_h \\ q_k \end{bmatrix}, \tag{22}$$

Let τ_a and τ_b be the external torques applied at pulley A and B, respectively. Let τ_h and τ_k be the external torques applied at the hip and knee. Then, the virtual work principle states

$$\tau_a \delta q_a + \tau_b \delta q_b + (-\tau_h)\, \delta q_h + (-\tau_k)\, \delta q_k = 0. \tag{23}$$

With $\delta q_a = \delta q_h - \gamma_a \delta q_k$ and $\delta q_b = \delta q_h + \gamma_b \delta q_k$, which are obtained from Eq. (22), Eq. (23) becomes

$$(\tau_a + \tau_b - \tau_h)\, \delta q_h + (-\gamma_a \tau_a + \gamma_b \tau_b - \tau_h)\, \delta q_k = 0. \tag{24}$$

Since Eq. (24) is satisfied for all δq_h and δq_k,

$$\begin{bmatrix} \tau_h \\ \tau_k \end{bmatrix} = \begin{bmatrix} 1 & 1 \\ -\gamma_a & \gamma_b \end{bmatrix} \begin{bmatrix} \tau_a \\ \tau_b \end{bmatrix}. \tag{25}$$

APPENDIX B
SYSTEM PARAMETERS

For friction force, Coulomb and viscous friction are modeled as follows.

$$\left(F_p\right)_i = \mu_i \tanh\left(\kappa \dot{q}_i\right) + \eta_i \dot{q}_i, \tag{26}$$

where μ_i is the coefficient of the Coulomb friction, η_i is the coefficient of the viscous friction, and κ is a positive constant. The friction parameters are identified based on the velocity-torque curves with no load, as shown in Fig. 11. Stiffness of timing belts are identified by measuring pulley torque while changing the pulley position where the joint positions are fixed. The timing belt is considered a linear spring and its stiffness is linearly fitted by the position-torque data, as shown in Fig. 12.

The actual parameters of the model dynamics are listed in Table 2. These model parameters are used for the feedback control in Eq. (19).

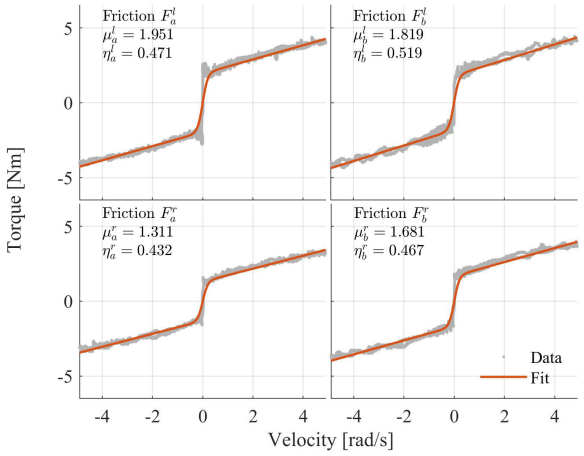

FIGURE 11. Friction of the belt-gear transmission on the driving pulleys. Each friction parameter is identified by measuring the actuator torque while changing its velocity. The measured data is fitted to a coulomb-viscous friction model in (26), where $\kappa = 5$.

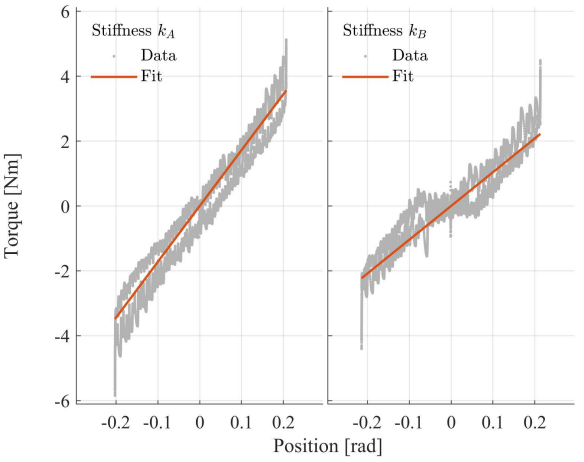

FIGURE 12. Stiffness of timing belts. The timing belt is considered a linear spring and its stiffness is linearly fitted by the position-torque data.

TABLE 2. Values of model parameters defined in Fig. 7.

Torso	α_u	0.506 rad	l_{uc}	0.178 m
	m_u	6.03 kg	I_u	0.0663 kg m^2
Thigh	l_t	0.4 m	l_{tc}	0.194 m
	m_t	0.942 kg	I_t	0.0246 kg m^2
Shank	l_s	0.4 m	l_{sc}	0.125 m
	m_s	0.49 kg	I_s	0.011 kg m^2
Pulley	m_a	0.243 kg	I_a	0.0147 kg m^2
	m_b	0.241 kg	I_b	0.0147 kg m^2
Cable	k_a	65.2 N m/rad	k_b	46.8 N m/rad

APPENDIX C
SYSTEM DYNAMICS

Refer to supplementary document "System dynamics.pdf".

REFERENCES

[1] Z. F. Lerner, D. L. Damiano, and T. C. Bulea, "The effects of exoskeleton assisted knee extension on lower-extremity gait kinematics, kinetics, and muscle activity in children with cerebral palsy," *Sci. Rep.*, vol. 7, no. 1, p. 13512, Dec. 2017.

[2] K. P. Michmizos, S. Rossi, E. Castelli, P. Cappa, and H. I. Krebs, "Robot-aided neurorehabilitation: A pediatric robot for ankle rehabilitation," *IEEE Trans. Neural Syst. Rehabil. Eng.*, vol. 23, no. 6, pp. 1056–1067, Nov. 2015.

[3] J. A. Blaya and H. Herr, "Adaptive control of a variable-impedance ankle-foot orthosis to assist drop-foot gait," *IEEE Trans. Neural Syst. Rehabil. Eng.*, vol. 12, no. 1, pp. 24–31, Mar. 2004.

[4] H. A. Quintero, R. J. Farris, and M. Goldfarb, "A method for the autonomous control of lower limb exoskeletons for persons with paraplegia," *J. Med. Devices*, vol. 6, no. 4, pp. 1–6, Dec. 2012.

[5] G. Zeilig, H. Weingarden, M. Zwecker, I. Dudkiewicz, A. Bloch, and A. Esquenazi, "Safety and tolerance of the ReWalk^{TM} exoskeleton suit for ambulation by people with complete spinal cord injury: A pilot study," *J. Spinal Cord Med.*, vol. 35, no. 2, pp. 96–101, Mar. 2012.

[6] L. E. Miller, A. K. Zimmermann, and W. G. Herbert, "Clinical effectiveness and safety of powered exoskeleton-assisted walking in patients with spinal cord injury: Systematic review with meta-analysis," *Med. Devices*, vol. 9, pp. 455–466, Mar. 2016.

[7] C. B. Baunsgaard, U. V. Nissen, A. K. Brust, A. Frotzler, C. Ribeill, Y.-B. Kalke, N. León, B. Gómez, K. Samuelsson, W. Antepohl, U. Holmström, N. Marklund, T. Glott, A. Opheim, J. Benito, N. Murillo, J. Nachtegaal, W. Faber, and F. Biering-Sørensen, "Gait training after spinal cord injury: Safety, feasibility and gait function following 8 weeks of training with the exoskeletons from Ekso Bionics," *Spinal Cord*, vol. 56, no. 2, pp. 106–116, Feb. 2018.

[8] *Ekso Bionics*. [Online]. Available: http://www.eksobionics.com

[9] *ReWalk Robotics*. [Online]. Available: http://www.rewalk.com

[10] *Cyberdyne*. [Online]. Available: http://www.cyberdyne.jp

[11] *Indego*. [Online]. Available: http://www.indego.com

[12] X. Jin, Y. Cai, A. Prado, and S. K. Agrawal, "Effects of exoskeleton weight and inertia on human walking," in *Proc. IEEE Int. Conf. Robot. Autom. (ICRA)*, May 2017, pp. 1772–1777.

[13] E. H. F. van Asseldonk, J. F. Veneman, R. Ekkelenkamp, J. H. Buurke, F. C. T. van der Helm, and H. van der Kooij, "The effects on kinematics and muscle activity of walking in a robotic gait trainer during zero-force control," *IEEE Trans. Neural Syst. Rehabil. Eng.*, vol. 16, no. 4, pp. 360–370, Aug. 2008.

[14] R. C. Browning, J. R. Modica, R. Kram, and A. Goswami, "The effects of adding mass to the legs on the energetics and biomechanics of walking," *Med. Sci. Sports Exerc.*, vol. 39, no. 3, pp. 515–525, Mar. 2007.

[15] L. Sykes, J. Edwards, E. S. Powell, and E. R. S. Ross, "The reciprocating gait orthosis: Long-term usage patterns," *Arch. Phys. Med. Rehabil.*, vol. 76, no. 8, pp. 779–783, Aug. 1995.

[16] M. Franceschini, S. Baratta, M. Zampolini, D. Loria, and S. Lotta, "Reciprocating gait orthoses: A multicenter study of their use by spinal cord injured patients," *Arch. Phys. Med. Rehabil.*, vol. 78, no. 6, pp. 582–586, Jun. 1997.

[17] J. Masood, J. Ortiz, J. Fernández, L. A. Mateos, and D. G. Caldwell, "Mechanical design and analysis of light weight hip joint parallel elastic actuator for industrial exoskeleton," in *Proc. 6th IEEE Int. Conf. Biomed. Robot. Biomechatronics (BioRob)*, Singapore, Jun. 2016, pp. 631–636.

[18] J. Choo and J. H. Park, "Increasing payload capacity of wearable robots using linear actuators," *IEEE/ASME Trans. Mechatronics*, vol. 22, no. 4, pp. 1663–1673, Aug. 2017.

[19] S. Jung, C. Kim, J. Park, D. Yu, J. Park, and J. Choi, "A wearable robotic orthosis with a spring-assist actuator," in *Proc. 38th Annu. Int. Conf. IEEE Eng. Med. Biol. Soc. (EMBC)*, Aug. 2016, pp. 5051–5054.

[20] S. Hirose and S. Ma, "Coupled tendon-driven multijoint manipulator," in *Proc. IEEE Int. Conf. Robot. Autom.*, Sacramento, CA, USA, Apr. 1991, pp. 1268–1275.

[21] I. M. C. Olaru, S. Krut, and F. Pierrot, "Novel mechanical design of biped robot SHERPA using 2 DOF cable differential modular joints," in *Proc. IEEE/RSJ Int. Conf. Intell. Robots Syst.*, St. Louis, MI, USA, Oct. 2009, pp. 4463–4468.

[22] J. F. Veneman, R. Kruidhof, E. E. G. Hekman, R. Ekkelenkamp, E. H. F. Van Asseldonk, and H. van der Kooij, "Design and evaluation of the LOPES exoskeleton robot for interactive gait rehabilitation," *IEEE Trans. Neural Syst. Rehabil. Eng.*, vol. 15, no. 3, pp. 379–386, Sep. 2007.

[23] X. Jin, X. Cui, and S. K. Agrawal, "Design of a cable-driven active leg exoskeleton (C-ALEX) and gait training experiments with human subjects," in *Proc. IEEE Int. Conf. Robot. Autom. (ICRA)*, May 2015, pp. 5578–5583. [Online]. Available: http://ieeexplore.ieee.org/document/7139979/

[24] Y. Ding, I. Galiana, A. T. Asbeck, S. M. M. De Rossi, J. Bae, T. R. T. Santos, V. L. de Araujo, S. Lee, K. G. Holt, and C. Walsh, "Biomechanical and physiological evaluation of multi-joint assistance with soft exosuits," *IEEE Trans. Neural Syst. Rehabil. Eng.*, vol. 25, no. 2, pp. 119–130, Feb. 2017.
[25] K. Kong, H. Moon, B. Hwang, D. Jeon, and M. Tomizuka, "Impedance compensation of SUBAR for back-drivable force-mode actuation," *IEEE Trans. Robot.*, vol. 25, no. 3, pp. 512–521, Jun. 2009.
[26] Y. Lee, Y.-J. Kim, J. Lee, M. Lee, B. Choi, J. Kim, Y. J. Park, and J. Choi, "Biomechanical design of a novel flexible exoskeleton for lower extremities," *IEEE/ASME Trans. Mechatronics*, vol. 22, no. 5, pp. 2058–2069, Oct. 2017.
[27] D. J. Hyun, H. Lim, S. Park, and S. Nam, "Singular wire-driven series elastic actuation with force control for a waist assistive exoskeleton, H-WEXv2," *IEEE/ASME Trans. Mechatronics*, vol. 25, no. 2, pp. 1026–1035, Apr. 2020.
[28] S. Lee, N. Karavas, B. T. Quinlivan, D. LouiseRyan, D. Perry, A. Eckert-Erdheim, P. Murphy, T. Greenberg Goldy, N. Menard, M. Athanassiu, J. Kim, G. Lee, I. Galiana, and C. J. Walsh, "Autonomous multi-joint soft exosuit for assistance with walking overground," in *Proc. IEEE Int. Conf. Robot. Autom. (ICRA)*, Brisbane, QLD, Austrailia, May 2018, pp. 2812–2819.
[29] J. Kim, G. Lee, R. Heimgartner, D. A. Revi, N. Karavas, D. Nathanson, I. Galiana, A. Eckert-Erdheim, P. Murphy, D. Perry, N. Menard, D. K. Choe, P. Malcolm, and C. J. Walsh, "Reducing the metabolic rate of walking and running with a versatile, portable exosuit," *Science*, vol. 365, no. 6454, pp. 668–672, 2019. [Online]. Available: http://science.sciencemag.org/content/365/6454/668.abstract
[30] J. Bae, C. Siviy, M. Rouleau, N. Menard, K. O'Donnell, I. Geliana, M. Athanassiu, D. Ryan, C. Bibeau, L. Sloot, P. Kudzia, T. Ellis, L. Awad, and C. J. Walsh, "A lightweight and efficient portable soft exosuit for paretic ankle assistance in walking after stroke," in *Proc. IEEE Int. Conf. Robot. Autom. (ICRA)*, Brisbane, QLD, Austrailia, May 2018, pp. 2820–2827.
[31] L. N. Awad, A. Esquenazi, G. E. Francisco, K. J. Nolan, and A. Jayaraman, "The ReWalk ReStore^{TM} soft robotic exosuit: A multi-site clinical trial of the safety, reliability, and feasibility of exosuit-augmented post-stroke gait rehabilitation," *J. NeuroEng. Rehabil.*, vol. 17, no. 1, p. 80, Dec. 2020.
[32] J. Park, S. Park, C. H. Park, S. Jung, C. Kim, J. H. Park, and J. Choi, "A robotic orthosis with a cable-differential mechanism," in *Proc. IEEE Int. Conf. Robot. Autom. (ICRA)*, Singapore, May 2017, pp. 517–521.
[33] R. W. Bohannon, "Knee extension power, velocity and torque: Relative deficits and relation to walking performance in stroke patients," *Clin. Rehabil.*, vol. 6, no. 2, pp. 125–131, May 1992.
[34] D. A. Winter, *Biomechanics and Motor Control of Human Movement*, 4th ed. Hoboken, NJ, USA: Wiley, 2009.

JAEHWAN PARK received the B.S. and M.S. degrees in mechanical engineering from Hanyang University, Seoul, South Korea, in 2010 and 2012, respectively, and the Ph.D. degree from the School of Mechanical Engineering, Hanyang University. In 2012 to 2015, he was a Researcher with the Korea Institute of Industrial Technology (KITECH), Ansan, South Korea. Since 2015, he has been working with the Korea Institute of Science and Technology (KIST), as a Student Researcher. His research interests include legged robots, cable-driven robots, and wearable robots.

SEUNGHAN PARK received the B.S. degree from the Department of Mechatronics Engineering, Korea Polytechnic University, Seheung-si, South Korea, in 2016, and the M.S. degree from the School of Mechanical Engineering, Korea University, Seoul, South Korea, in 2018. Since 2018, he has been working as a Student Researcher with the Korea Institute of Science and Technology (KIST). His research interests include rehabilitation robot design, wearable exoskeleton robots, variable stiffness actuator, and human–machine interaction.

CHANKYU KIM received the B.S. degree in robotics from Kwangwoon University, Seoul, South Korea, in 2017. He was with the Korea Institute of Science and Technology (KIST), Seoul, from 2017 to 2019. His research interests include robotics and embedded system design.

JONG HYEON PARK (Member, IEEE) received the B.S. degree in mechanical engineering from Seoul National University, Seoul, South Korea, in 1981, and the M.S. and Ph.D. degrees from the Massachusetts Institute of Technology (MIT), Cambridge, MA, USA, in 1983 and 1991, respectively. Since 1992, he has been with the School of Mechanical Engineering, Hanyang University, Seoul, where he is currently a Professor. He was with Korea Science and Engineering Foundation Japan Society for the Promotion of Science. He was a Visiting Researcher at Waseda University, Tokyo, Japan, in 1999; a KOSEF-CNR Visiting Researcher at the Scuola Superiore Sant'Anna, Pisa, Italy, in 2000; a Visiting Scholar at MIT, in 2002 to 2003; and a Visiting Scholar at Purdue University, West Lafayette, IN, USA, in 2008 to 2010. He was also associated with Brooks Automation Inc., Chelmsford, MA, USA, in 1991 to 1992 and 2001 to 2002. His research interests include biped robots, robot dynamics and control, haptics, and biorobots. Since 2010, he has been serving as a Senior Editor of the *Journal of Mechanical Science and Technology*. He is a member of The Korean Society of Mechanical Engineers, The Korean Society of Automotive Engineers, Korean Society of Precision Engineering, and Institute of Control, Robotics and Systems.

JUNHO CHOI (Member, IEEE) received the B.S. degree in electrical engineering from Hanyang University, Seoul, South Korea, in 2000, and the Ph.D. degree in electrical engineering systems from the University of Michigan, Ann Arbor, in 2005. He is with the Center for Bionics, the Korea Institute of Science and Technology, Seoul, where he is currently a Principal Research Scientist. His research interests include nonlinear control, bipedal robot control, design and control of robots, and orthoses for gait rehabilitation and assistance.